Presented at the ASM/OTA/FMS Conference:
Materials Substitution: Availability,
Energy and Environmental Factors, Chicago, IL,
September 27 - 28, 1977; also Submitted to
Metals Progress

LBL-7397
c.2

THE DEVELOPMENT OF NICKEL-FREE AUSTENITIC STAINLESS STEELS FOR AMBIENT AND CRYOGENIC APPLICATIONS

Glen T. Haddick, Larry D. Thompson,
Earl R. Parker, and Victor F. Zackay

February 1978

Prepared for the U. S. Department of Energy
under Contract W-7405-ENG-48

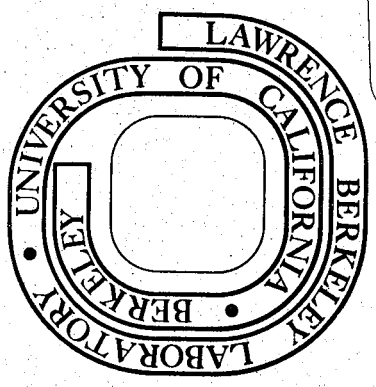

LBL-7397
c.2

Presented at the ASM/OTA/FMS Conference:
MATERIALS SUBSTITUTION: AVAILABILITY,
ENERGY AND ENVIRONMENTAL FACTORS, Chicago,
September 27-28, 1977 and submitted to
Metals Progress.

THE DEVELOPMENT OF NICKEL-FREE AUSTENITIC STAINLESS STEELS FOR AMBIENT AND CRYOGENIC APPLICATIONS

Glen T. Haddick*, Larry D. Thompson+, Earl R. Parker* and Victor F. Zackay*

Materials and Molecular Research Division, Lawrence Berkeley Laboratory
and Department of Materials Science and Mineral Engineering
University of California, Berkeley, California 94720

February 1978

---

* Graduate student and Professors of Physical Metallurgy, respectively, Department of Materials Science and Mineral Engineering, University of California, Berkeley, California 94720.
+ Formerly a graduate student in the Department of Materials Science and Mineral Engineering now with General Atomic Company, San Diego, California 92121.

THE DEVELOPMENT OF NICKEL-FREE AUSTENITIC STAINLESS STEELS FOR AMBIENT AND CRYOGENIC APPLICATIONS

Glenn T. Haddick, Larry D. Thompson, Earl R. Parker and Victor F. Zackay

Materials and Molecular Research Division, Lawrence Berkeley Laboratory
and Department of Materials Science and Engineering
University of California, Berkeley, California 94720

ABSTRACT

A series of alloys have been developed as possible replacements for some austenitic stainless steels. These alloys utilized a Mn substitution for Ni and a reduced Cr concentration from the 18% ordinarily found in the AISI 300 series stainless steels to a concentration of 13%. The base system studied was an alloy containing Fe-16%Mn-13%Cr while other elements added included small additions of N, Si and Mo. A range of microstructures was produced from the alloying additions. The base composition had a triplex (fcc, hcp, bcc) structure while the most highly modified compositions were fully austenitic.

Mechancical testing included tensile testing and Charpy V-notch testing conducted at various temperatures between -196°C to 23°C. Excellent combinations of strength and ductility were obtained (40-65 ksi yield strength, 100-125 ksi ultimate strength, 45-75% elongation and 60-80% reduction of area) at room temperature. Upper shelf energies in Charpy V-notch testing were as high as 185 ft-lbs. with a ductile-brittle transition temperature (DBTT) of

-160°C. Analysis of fracture surfaces determined that alloys without interstitials had no transition in the mode of failure between room temperature and liquid nitrogen temperature. Results of an ASTM sensitization corrosion test, where the experimental alloys were compared to 347 stainless steel, indicated that the alloys were not susceptible to intergranular attack.

INTRODUCTION

The motivation behind this research was to develop new stainless alloys which had comparable properties to standard AISI 300 series stainless steels and also utilized less of the critical elements, Cr and Ni. Much has been made in the press about our country's dependence upon foreign sources of raw materials that are necessary for a healthy economy. The oil embargo of 1973 was the most dramatic example of this dependence and the resulting economic ramifications. The importation of metals holds a similar potentiality of problems to the manufacture and utilization of stainless steels. Therefore, it was felt that research into the design of new stainless steels was needed to meet changing world conditions and our country's changing technological requirements. The Fe-Mn-Cr system provided a good alternative to standard stainless steels. In fact, the Fe-Mn-Cr based systems possessed better ambient temperature properties than standard AISI 300 series stainless steels with the advantages of not requiring Ni and reduced Cr levels. A short synopsis of previous work on the Fe-Mn-Cr system is in order to lead directly into the work presented here.

Schanfein[1] and Thompson[2] have studied the effect of Cr additions on the microstructure and mechanical properties of Fe-Mn binary alloys. Schanfein studied additions of 8%Cr to Fe-Mn alloys containing from 12% to 20% Mn, while Thompson looked at additions of 13% and 18% Cr in Fe-Mn alloys containing from 14% to 20% Mn. The alloys of both investigations were ice-brine quenched and refrigerated in liquid nitrogen after a 900°C austenitization in air. The results indicated that increasing amounts of Cr in the Fe-16%Mn alloy increased the yield and ultimate strengths over the entire temperature range tested (i.e. -196°C to 23°C) while the ductility remained

relatively constant. The ductile-brittle transition temperature (DBTT) was unaffected by the additions of Cr, however the energy absorbed at any one temperature decreased with increasing amounts of Cr. In one heat treatment varient, air cooling instead of quenching, the Fe-16%Mn-13%Cr alloy showed an increase of 60 ft-lbs. in the Charpy V-notch energy over the entire temperature range when compared to the quenched alloy. The mechanical properties were found to depend, in part, on the types of microstructure produced from the changes in chemical composition and heat treatment.

The Fe-16%Mn-13%Cr alloy was chosen as the base alloy for this investigation because it possessed the best combination of strength, ductility and impact resistance. Likewise, air cooling was chosen as the heat treatment for its simplicity, commercial acceptability and the previously mentioned improvement in impact resistance. N was chosen as a strengthening agent and austenite former because when in the sensitized condition where C is added for this purpose it can lead to embrittlement[3]. C also causes poor corrosion resistance in stainless steels when Cr-carbides form preferentially near grain boundaries. Further additions of Si and Mo were made for strengthening and improving general corrosion resistance. The effect of chemical modifications on the microstructure will be discussed followed by an assessment of the mechanical properties. The substructure of these alloys will be presented and the corrosion resistance will be established by several general tests.

EXPERIMENTAL PROCEDURE

The alloys used in this investigation were melted in a vacuum induction furnace into which were put high purity (99.9+%) Fe, Mn, Cr, Mo and Si. N was added to the alloys by flushing and backfilling the furnace with N. Table I shows the analyzed chemical compositions of the alloys. After the elements were melted in a zirconia crucible, twenty pound ingots were cast in 3 inch diameter Cu chill molds and furnace cooled. The ingots were then homogenized at 1200°C for twenty-four hours in an Ar atmosphere followed by furnace cooling. Next, the ingots were upset and crossforged at 1200°C in air to a crossection of 2-3/4 inches wide by 1/2 inch thick followed by air cooling.

After forging, the bars were cut to suitable lengths for specimen preparation and then heat treated. The heat treatment consisted of austenitizing at 900°C in air for two hours followed by air cooling. The only exception to this procedure was carried out for alloy III which contained Mo and N, and the air cool resulted in nitrides being formed at grain boundaries. Alloy III was ice water quenched to avoid these precipitates.

The mechanical tests used in this investigation were tensile tests at three different temperatures: -196°, -78°, 23°C, and Charpy V-notch impact tests at a variety of temperatures between -196° and 23°C. ASTM standard (E8-69 and E23-72) specimens.were used for both types of testing. Table II shows the tensile test properties of the alloys, where two tests were used for each point. The fracture mechanisms were identified using scanning electron microscopy.

Metallography was accomplished using several techniques. Optical microscopy specimens were prepared in a conventional manner by grinding

and polishing followed by electropolishing. Alloys with mixed microstructures electropolished best in a solution of 75 gm CrO_3 plus 400 ml glacial acetic acid plus 20 ml distilled water, while the austenitic alloys were electropolished in oxalic acid. The specimens were etched in a mixed acids solution containing 11 ml HCl, 5 ml HNC_3 and 11 ml H_2O. Optical microscopy was compared to X-ray diffraction phase analysis which was done on a Picker X-ray diffractometer using Cr K_α radiation. Phases were identified by comparing the integrated intensities of the (200) and (211) alpha peaks, the (220) and (311) austenite peaks and the (01.2) epsilon peak. A quantitiative volume fraction analysis for a three phase microstructure is given in Cullity[4]. The substructure of these alloys was determined using transmission electron microscopy. 3 mm diameter discs were chemically thinned in an Hf-H_2O_2 solution followed by jet polishing in a solution containing nitric acid and methanol at -30°C. Specimens were examined using a JEM 7A transmission electron microscope operated at 100 KV.

Several general corrosion tests were also employed to characterize the resistance of these steels to environmental attack. An air oxidation test and an ASTM sensitization immersion corrosion test were two specific tests used to characterize the materials. In these tests, the experimental alloys were compared to AISI 347 stainless steel. An EDAX (energy dispersive analysis of x-rays) technique was employed to detect chemical composition variances across phase boundaries and grain boundaries in optical metallography samples prepared from corrosion specimens.

RESULTS AND DISCUSSION

A. Chemical Composition and Microstructure

Table I shows the nominal chemical compositions of the alloys used in this investigation. The base composition of Fe-16%Mn-13%Cr (alloy I) was modified by additions of 0.13%N (alloy II), 1.5%Si + 0.2%N (alloy III), or 2%Mo + 0.2%N (alloy IV). Table I also shows the volume percentages of phases present in each alloy which were determined by x-ray analysis. The base alloy was found to be a three-phase mixture of face centered cubic austenite (γ), hexagonal close-packed epsilon martensite (ε), and body centered cubic alpha (α), and its microstructure is shown in Figure 1. Epsilon martensite occurred in relatively thick bands while the alpha formed at an angle across the epsilon martensite band, and typically had a lens shaped morphology (see the arrow in Figure 1). While the etchant used here did not in itself distinguish between the three phases present, other investigators have reported similar morphologies in Fe-Mn alloys[1-3,5].

Epsilon martensite has been studied in Fe-Mn-C alloys by Gordon-Parr[6] and Schumann[7]. It was found that epsilon martensite had a hexagonal crystal structure ($a/a = 1.61$) which had a 2.1% volume decrease from the volume occupied by the austenite (alpha had a 2.7% volume increase from austenite). These investigators also found that epsilon martensite characteristically formed in thin bands (parallel to the (111) austenite planes) which in some cases extended across an entire austenite grain. Epsilon martensite also grew by thickening perpendicular to the basal plane. More will be said later about the connection between twinning and epsilon martensite and stacking faults which can act as nucleation sites for the phase transformations in these alloys.

Figure 2 shows the microstructure of the Fe-16%Mn-13%Cr-0.13%N alloy which had a phase composition of 87% austenite and 13% epsilon martensite.

Thinner bands of epsilon martensite were present as well as a larger grain size than alloy I. Figure 3 shows the microstructure of alloy IV which has characteristic of both austenitic alloys with equiaxed grains and annealing twins.

One notices from table I that as the alloy content increased, the phases present in the alloys tended toward austenite. This trend has been attributed to the N additions since Si and Mo are know ferrite stabilizers.

B. Mechanical Properties

The mechanical properties of the alloys in tension are listed in table II while some specific variations in these properties are shown in Figures 4 and 5.

The variation of tensile test properties for all the alloys tested at room temperature is shown in Figure 4. The top graph depicts the yield and ultimate strengths while the bottom graph shows the percentages of elongation and reduction of area. Alloy I which had the three phase microstructure, had a yield strength of 45 ksi, an ultimate strength of 100 ksi with elongation and reduction of area of 43% and 80% respectively. Alloy II had a yield strength of 46 ksi, and ultimate strength of 120 ksi and an elongation and reduction of area of 70% and 78% respectively. The effect of the 0.13%N addition was twofold. First, the expected solid solution strengthening from the N addition was not apparent from the observed properties which can be explained by the larger grain size and increasing proportions of austenite in alloy II. Secondly, the elongation and ultimate strength increased significantly in alloy II, and was due to the mechanical stabilizing effect of N and increased the strain hardening capacity of the metastable γ and ε phases. This type of behavior has been noted before[3], where an austenite stabilizing element (eg. C) added to a mechanically metastable alloy (i.e., an alloy with

a stress or strain-induced phase transformation) increased both of these properties.

These increases in ultimate strength and elongation have been attributed to the effect of the alloying addition on the relative position of the M_s and M_d temperatures with respect to the test temperature (in this case, room temperature). Optimum properties in a metastable alloy are achieved when the test temperature is fixed somewhere in the middle of the M_s-M_d temperature range by the alloying elements. When this occurs, a small amount of the transformation product strengthens the alloy during each increment of strain until failure. However, when the test temperature is close to the M_s temperature, too much of the transformation product is produced with the first increments of strain and the alloy fails by premature necking because the transformation (strengthening) ceases to be effective at higher strains. Alternatively, when the test temperature is very close to the M_d temperature (that temperature, above which, no amount of strain can induce the transformation) not enough transformation strengthening occurs to prevent premature failure by necking. Therefore, a balance in chemical composition of a metastable alloy leads to optimum properties.

Alloys III and IV showed significant increases in yield strength and only nominal increases in ultimate strength or percent elongation. The increase in yield strength was attributed to solid solution strengthening of the extra N and the addition of either Si or Mo. Similarly, the addition of all of these elements contributed to the mechanical stability of the alloys and maintained the high ultimate strength and ductility.

Figure 5 shows how the test temperature effects the ductility of the alloys. In all of the alloys except alloy I, the ductility (both reduction of area and percent elongation) was reduced when testing occured at liquid nitrogen temperature. The conclusion drawn here was that, at -196°C, the

epsilon martensite, which had interstitial N, was embrittled in alloys II, III, IV and that the embrittled strain induced epsilon martensite could act as crack nucleation sites. This conclusion was reasonable because of the lattice contraction upon formation of ε martensite and was confirmed by scanning electron fractographs and by Charpy V-notch testing.

The impact properties of the alloys were studied using Charpy V-notch tests conducted in the temperature range -196°C to 23°C, and the results of these tests are shown in Figure 6. Alloy I had an upper shelf energy of 135 ft-lbs. which decreased gradually with decreasing temperature. The shape of the curve corresponds very closely to that of an Fe-16%Mn binary alloy[1], and was typical of three-phase microstructures with low interstitial content. SEM fractographs of alloy I, Figure 7, showed that there was no change in the mode of fracture between 23°C and -196°C, and that the fracture could be characterized as ductile, microvoid coalescence.

Alloy II showed a flat upper shelf of 185 ft-lbs. which extended down to -78°C before showing any embrittlement. The flat upper shelf was characteristic of a more stable austenite than alloy I. The role of epsilon martensite in the mode of fracture of alloy II at -196°C was evident from the SEM fractograph shown in Figure 8. The bottom photograph shows an enlargement of an area where fracture proceeded along epsilon martensite plates. Alloys III and IV showed behavior indicative of higher interstitial contents. All of the alloys had a DBTT at or below -100°C and impact energies better than 75 ft-lbs. at the DBTT.

The next three figures (i.e. 9, 10 and 11) are examples of the substructure of the alloys examined in the transmission electron microscope. Figure 9 shows a typical austenitic substructure in this Fe-Mn-Cr system.

One important feature was the overlapping stacking faults seen at 'A' in the figure. The stacking faults were indicative of low stacking fault energies and shed some light on how epsilon martensite could form in these alloys. Dislocation theory explains that the formation of stacking faults on every other (111) austenite plane leads to a hexagonal structure. Twinning takes place when stacking faults pass through an austenite structure on every (111) plane. Thus, it seems likely that epsilon martensite could form in regions like 'A' in Figure 9 where there are many overlapping stacking faults. The other important feature of this substructure was that there were stacking faults on intersecting (111) planes shown at 'B'. Figure 10 shows an alpha martensite lens (at 'A') which had grown in a band of epsilon martensite (B) which had transformed from austenite (C). The specimen was prepared from one of the austenitic alloys (III or IV) which was cooled to -196°C. Thus, Figure 10 showed that alpha martensite could form athermally at the intersection of a phase boundary and a stacking fault (D). One thing noted in the figure was the heavily faulted nature of the epsilon phase. Figure 11 shows a deformed structure taken from a tensile specimen where the dark bands in the figure were epsilon martensite, the light areas in between the bands corresponded to austenite and the light irregularly shaped phase at the intersections of the epsilon martensite bands was alpha martensite.

C. Corrosion Properties

In all of the corrosion tests reported here, the corrosion rates were calculated from weight losses which were converted to penetration rates. Also, the four experimental alloys were compared to 347 stainless steel in all of the tests.

Figure 12 shows the results of an oxidation in air test conducted

at 1100°C for 136 hours. The ordinate shows the penetration rate in mils/month (0.001 in./month) while the abscissa lists the five steels tested. The test is qualitative in that above 1000°C, the Cr_2O_3 layer that forms on stainless steels can be further oxidized to a volitile CrO_3 compound. The experimental alloys were never intended to be used anywhere near the conditions of this test, however, the test did show how the experimental alloys compared with 347 stainless steel containing 4 to 6% more Cr and 11% more Ni. 347 stainless steel exhibited an oxidation rate of 30 mils/month while alloys I, II and III showed somewhat slower penetration rates. In fact, alloy III showed a penetration rate of just 5 mils/month. No explanation was advanced for the poor performance of alloy IV.

Figure 13 shows the data collected from an immersion test in a boiling solution of 6M NH_4F + 0.5M NH_4No_3 which was conducted for 24 hours. This solution is used to declad Zircaloy fuel rods for the nuclear power industry and as such, it is a severe test of a material's resistance to attack. 347 stainless steel showed a penetration rate of 40 mils/month while all of the experimental alloys showed a lower rate of attack. Alloy III showed a corrosion rate of 20 mils/month.

Figure 14 shows the results of the test used to detect a material's susceptibility to sensitization. The test utilized a boiling solution containing 6M HNO_3 + 0.01M CrO_3 and was conducted for 48 hours. All the alloys were tested in this solution in the annealed condition as well as 347 stainless steel and alloys I and III in the sensitized condition. The standard ASTM sensitization treatment was used which comprised a one hour heat treatment at 1200°F followed by water quenching. The shaded bars in Figure 14 show the performance of the alloys in the sensitized condition. Alloys I and

III were found to perform at three times the level as that observed by 347 stainless steel in the sensitized condition even though 347 stainless steel was stabilized by the addition of Nb which reduces carbide precipitation at grain boundaries. The reason that alloys I and III performed better was that these alloys contained no C and were not supposedly susceptible to reductions in Cr content near the grain boundaries. In fact, alloy III was heat treated by initially air cooling which produced Mo-nitrides in the grain boundaries. Figure 15 shows micrographs of alloy III which were prepared by sectioning perpendicular to the attacked surface and showed that there was no preferential attack in the grain boundaries even with nitrides in the grain boundaries. The composition variation of Cr across grain boundaries was checked using an EDAX technique and was not found to have significant variations across grain boundaries.

CONCLUSIONS

1. N was an effective austenite former.
2. Additions of Mo, Si and particularly N contributed to the mechanical stability and increased the strain hardening capacities of the alloys which resulted in the high ductility observed during tensile testing.
3. Interstitials embrittled the alloys at -196°C and fracture was observed to occur along epsilon martensite plates.
4. Small additions of N raised the upper shelf energy in a Charpy V-notch test but also raised the DBTT.
5. Strain-induced alpha martensite was observed to form at intersections of epsilon martensite plates.
6. Corrosion studies indicated that two of the experimental alloys were not susceptible to sensitization-induced intergranular attack and that the experimental alloys were comparable to 347 stainless steel under several different conditions.

ACKNOWLEDGEMENT

The authors wish to express their gratitude to the Department of Energy (formerly the Energy Research and Development Administration) for the support of this research. We also extend our thanks to the Battelle Pacific Northwest Laboratory for conducting the corrosion tests reported herein.

REFERENCES

1. M. J. Schanfein, M. S. Thesis, U. C. Berkeley, "The Cryogenic Properties of Fe-Mn and Fe-Mn-Cr Alloys", LBL-2749.
2. L. D. Thompson, "The Mechanical Properties and Microstructural Relationships in Fe-Mn-Cr Alloys", M. S. Thesis, U. C. Berkeley, LBL-6232.
3. G. T. Haddick, "Optimization of Strength and Ductility in Fe-Mn TRIP Steels", M. S. Thesis, U. C. Berkeley, LBL-3986.
4. B. D. Culity, "Elements of X-Ray Diffraction", Addison-Wesley, California, 1956, pp. 388-396.
5. K. Sipos, L. Remy, A. Pineau, Met. Trans. 7A, June 1976, p. 857.
6. J. Gordon-Parr, Ac-a Crys., 5, (1952), p. 842.
7. H. Schumann, Arch. Eisenh., 38, 1967, pp. 647-656.

Table 1. Influence of Composition on Volume Percent Phases Present

Alloy	γ	ε	α
16 Mn - 13 Cr	31	33	36
16 Mn - 13 Cr - 0.13 N	83	17	0
16 Mn - 13 Cr - 0.2 N - 2 Mo	100	0	0
16 Mn - 13 Cr - 0.2 N - 1.5 Si	100	0	0

FIGURE CAPTIONS

1. Optical microstructure of Fe-16%Mn-13%Cr alloy.
2. Optical microstructure of Fe-16%Mn-13%Cr-0.13%N alloy.
3. Optical microstructure of Fe-16%Mn-13%Cr-1.5%Si-0.2%N alloy.
4. Room temperature tensile test properties of the experimental alloys.
5. Ductility vs. test temperature of the experimental alloys.
6. Ductile-Brittle Transition Temperature curves for the experimental alloys.
7. Scanning electron micrograph of alloy I: a) @ room temperature, b) @ -196°C.
8. Scanning electron micrograph of alloy II: a) and b)@ -196°C.
9. Transmission electron micrograph of alloy III showing 'A': overlapping stacking faults and 'B': faults on intersecting (111) planes.
10. Transmission electron micrograph of alloy III cooled to -196°C showing 'A': alpha martensite lens, 'B': epsilon martensite plate, 'C': austenite, 'D': stacking fault.
11. Transmission electron micrograph of alloy II after tensile deformation.
12. Oxidation in air test results.
13. Test results of test in boiling 6M NH_4F + 0.5M NH_4NO_3.
14. Sensitization corrosion test results for 347 stainless steel and the experimental alloys.
15. Optical micrograph of alloy III in the sensitized condition after testing showing nitrides in the grain boundaries and the absence of preferential attack.

XBB 768-7774

Figure 1.

XBB 768-7767

Figure 2.

XBB 768-7768

Figure 3

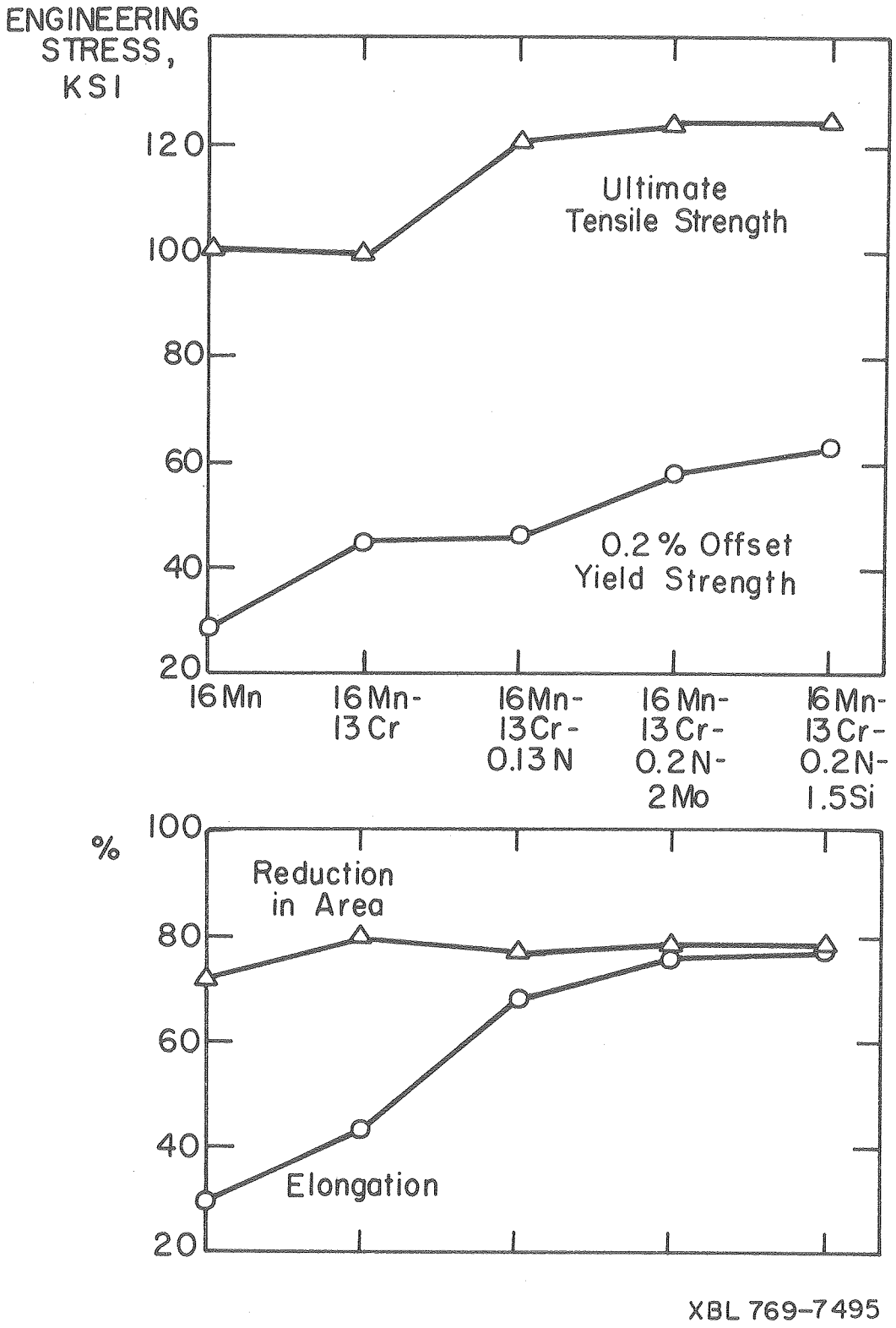
ENGINEERING STRESS, KSI
120
100
80
60
40
20
Ultimate Tensile Strength
0.2 % Offset Yield Strength
16 Mn
16 Mn-13 Cr
16 Mn-13 Cr-0.13 N
16 Mn-13 Cr-0.2 N-2 Mo
16 Mn-13 Cr-0.2 N-1.5 Si
%
100
80
60
40
20
Reduction in Area
Elongation
XBL 769-7495

Figure 4.

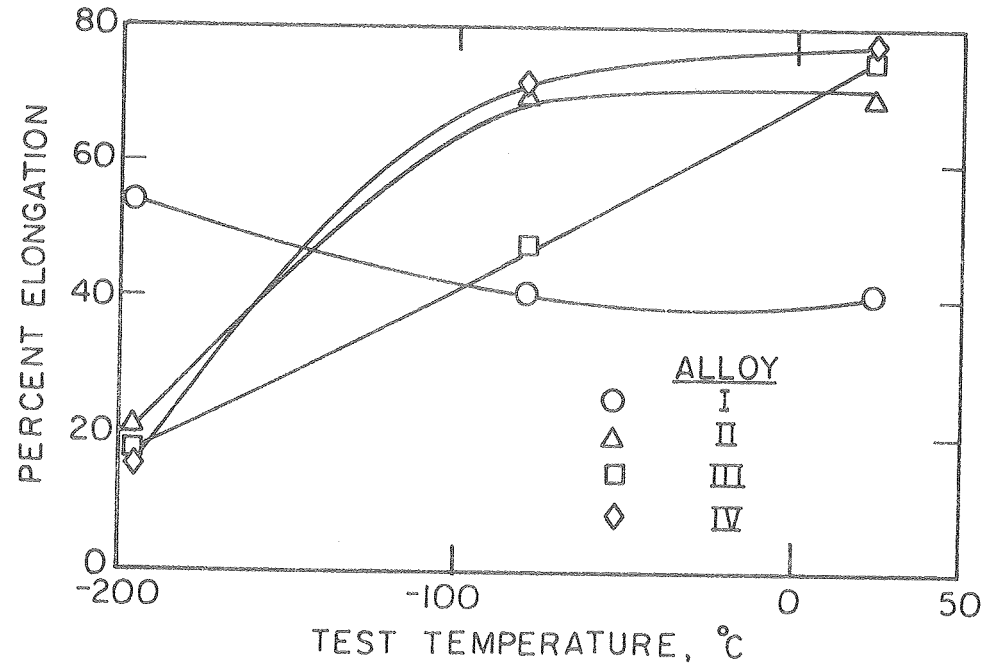

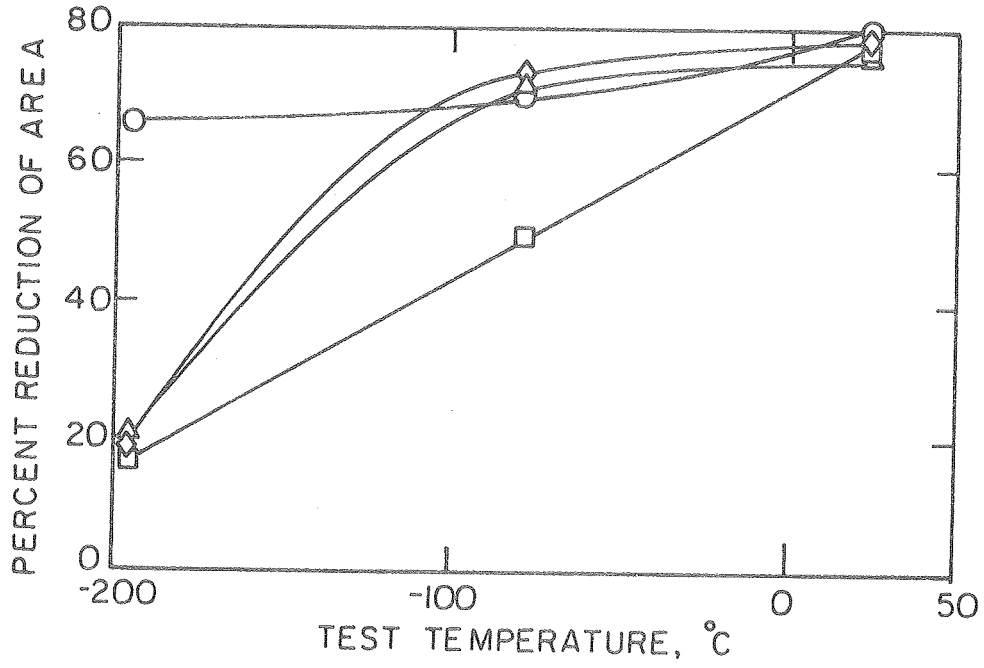

XBL782-4577

Figure 5.

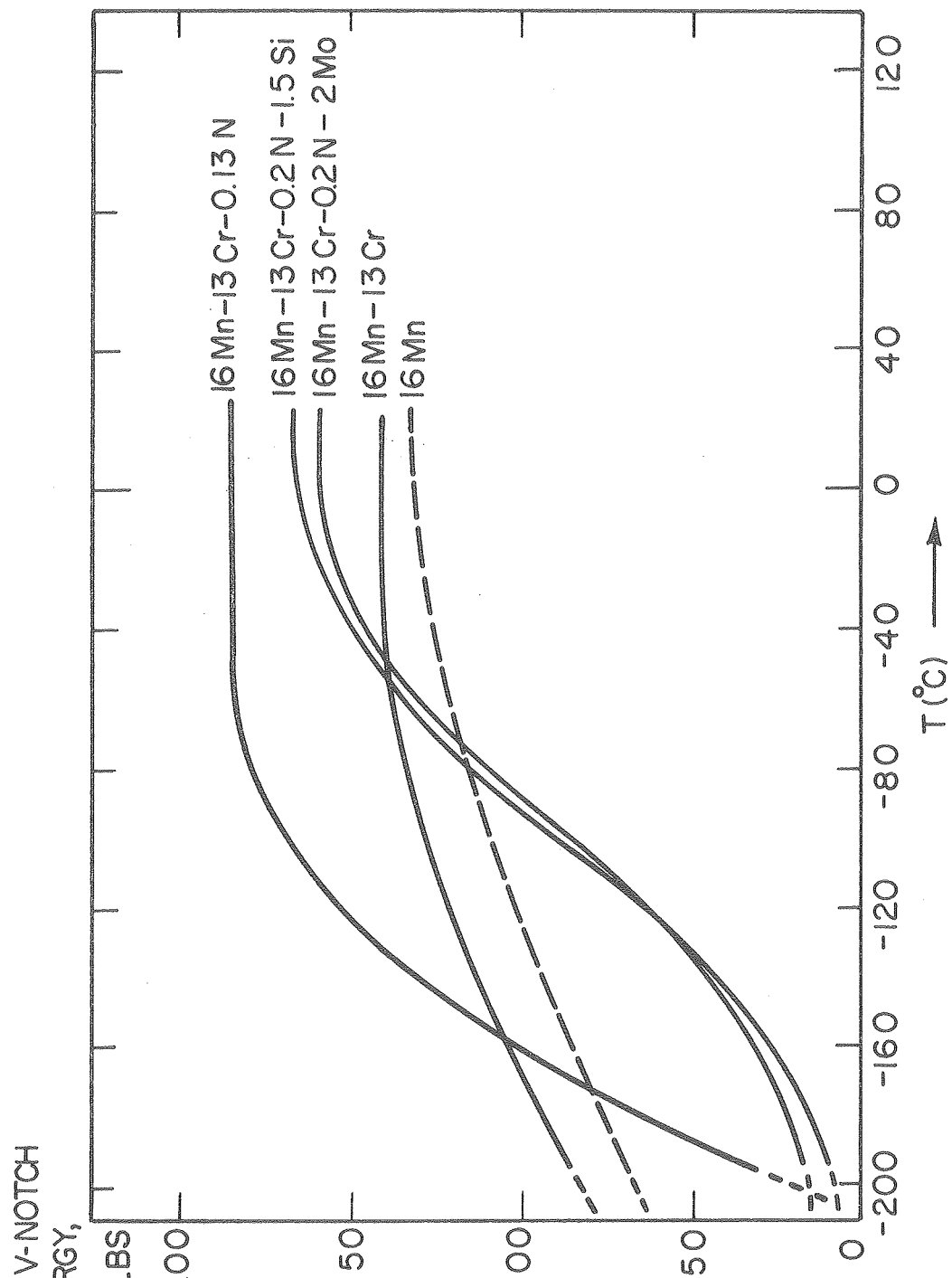

XBL 769-7494

Figure 6.

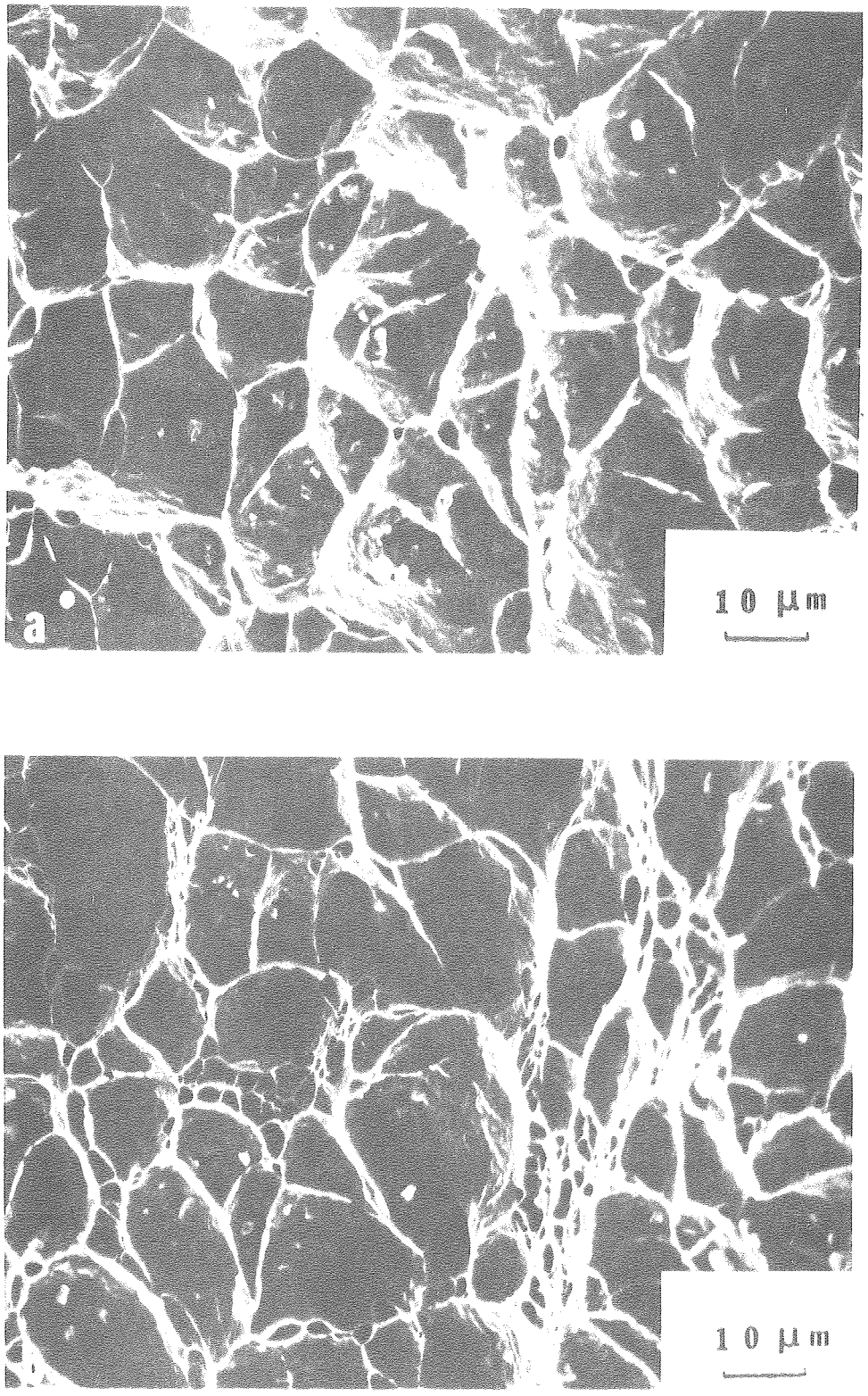

XBB 768-7754

Figure 7.

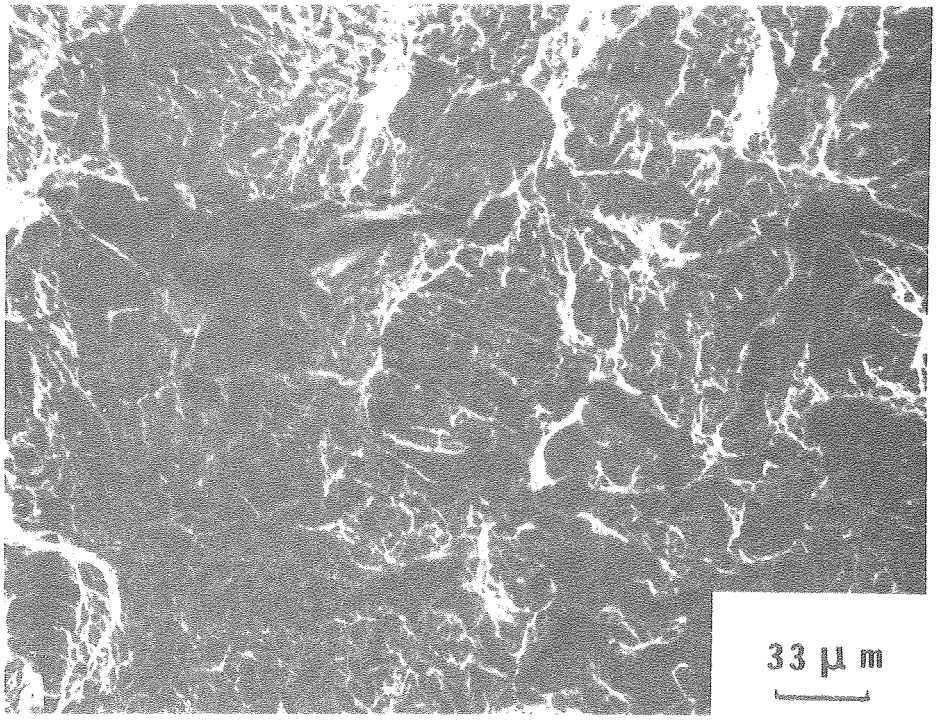

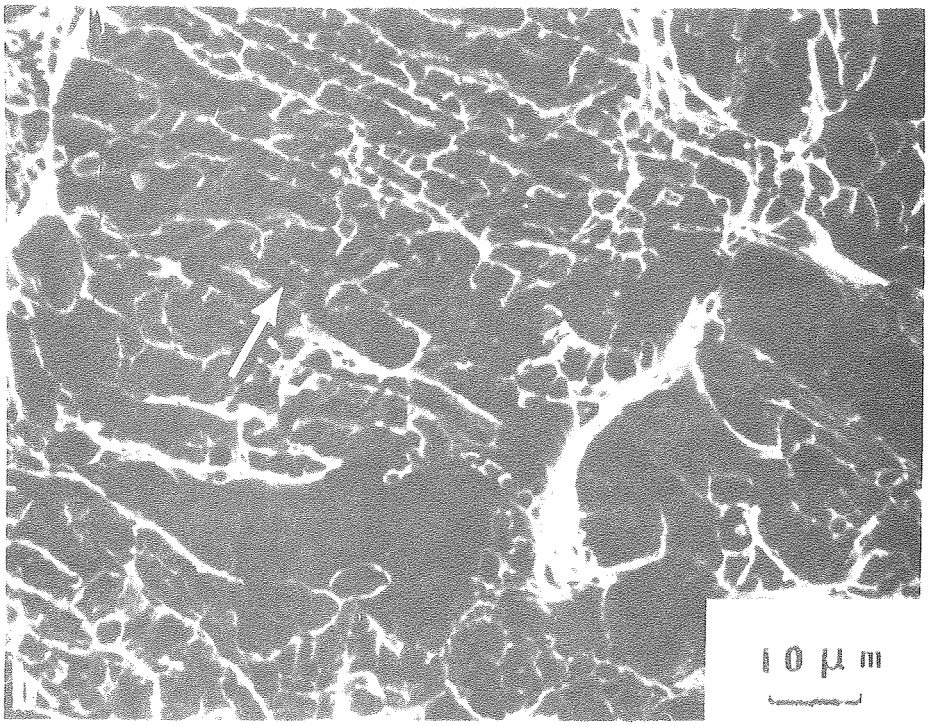

XBB 768-7752

Figure 8.

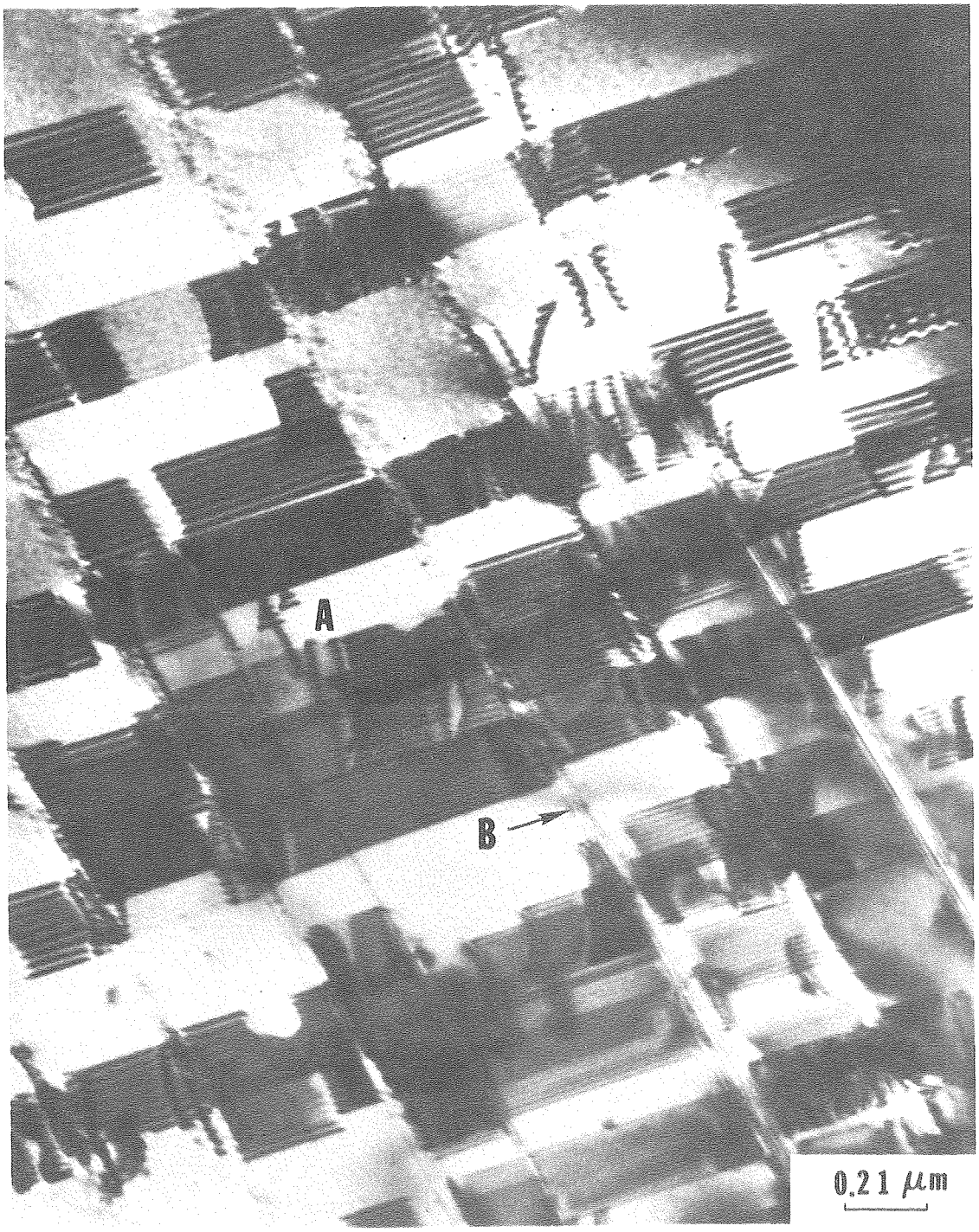

XBB 779-8901

Figure 9.

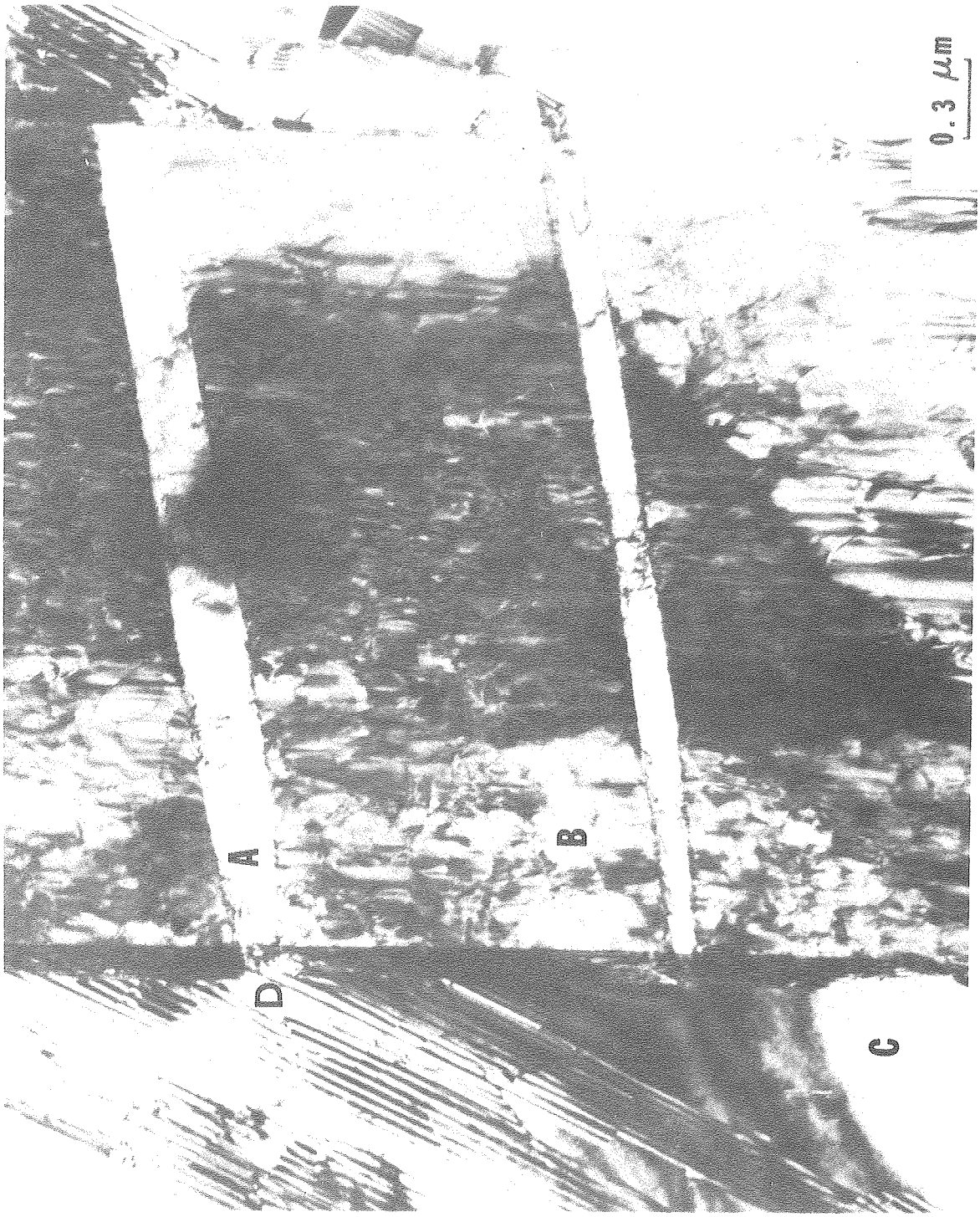

XBB 779-8900

Figure 10.

XBB 779-8902

Figure 11.

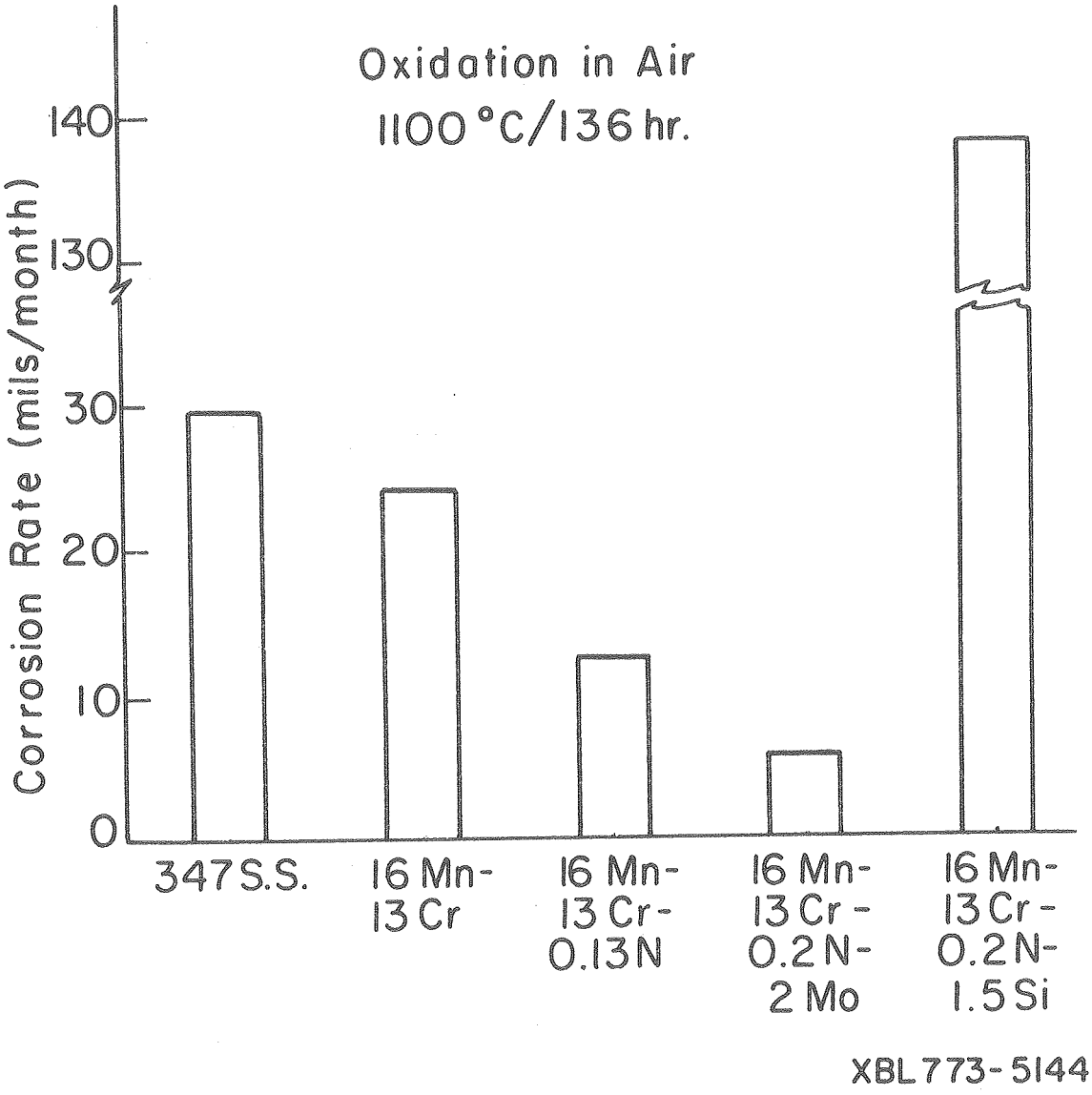
Oxidation in Air
1100 °C/136 hr.
Corrosion Rate (mils/month)
140
130
30
20
10
0
347 S.S.
16 Mn-13 Cr
16 Mn-13 Cr-0.13N
16 Mn-13 Cr-0.2N-2 Mo
16 Mn-13 Cr-0.2N-1.5 Si
XBL773-5144

Figure 12.

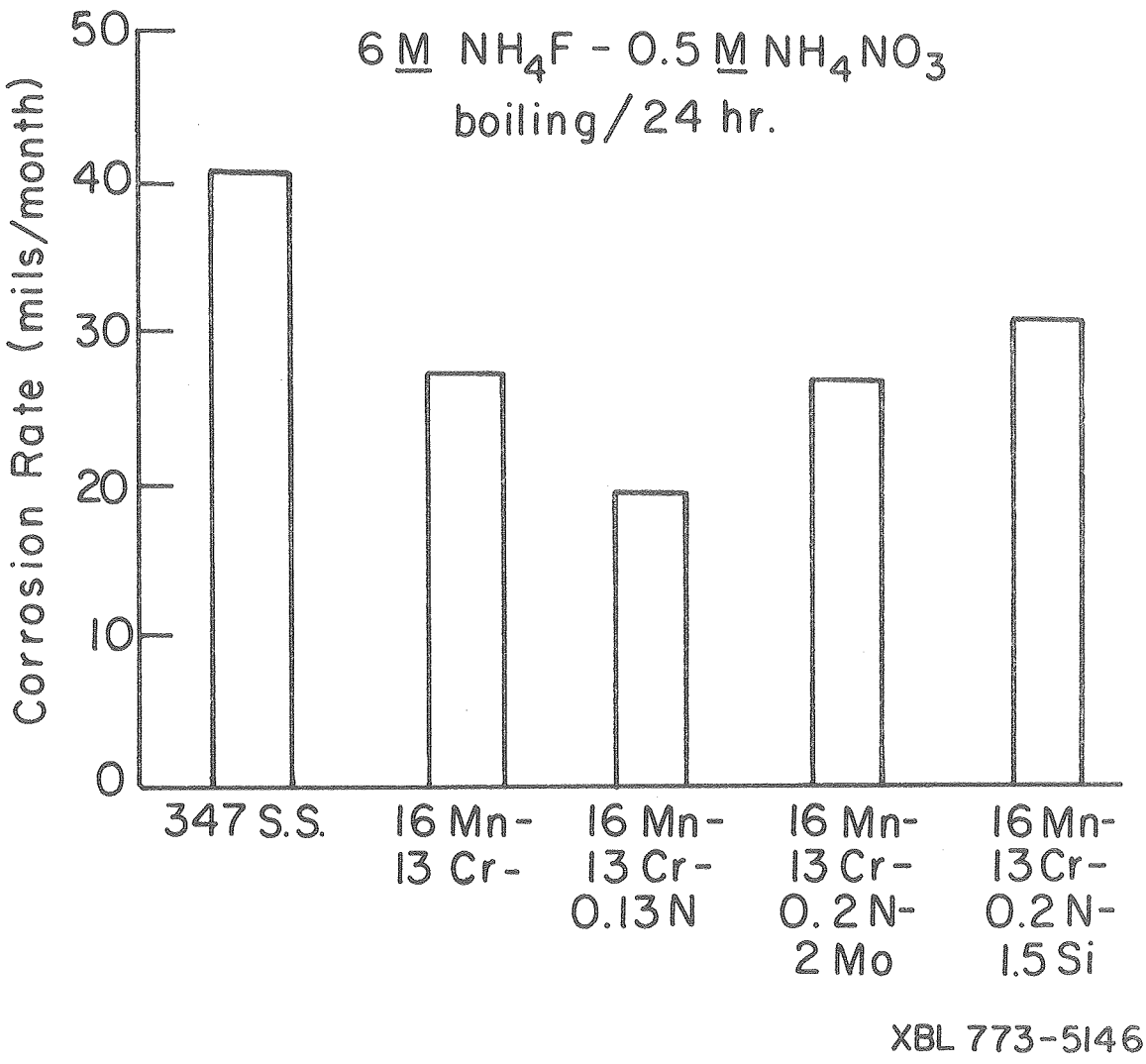
6 M NH_4F - 0.5 M NH_4NO_3
boiling / 24 hr.
Corrosion Rate (mils/month)
50
40
30
20
10
0
347 S.S.
16 Mn-13 Cr-
16 Mn-13 Cr-0.13N
16 Mn-13 Cr-0.2N-2 Mo
16 Mn-13 Cr-0.2N-1.5 Si
XBL 773-5146

Figure 13.

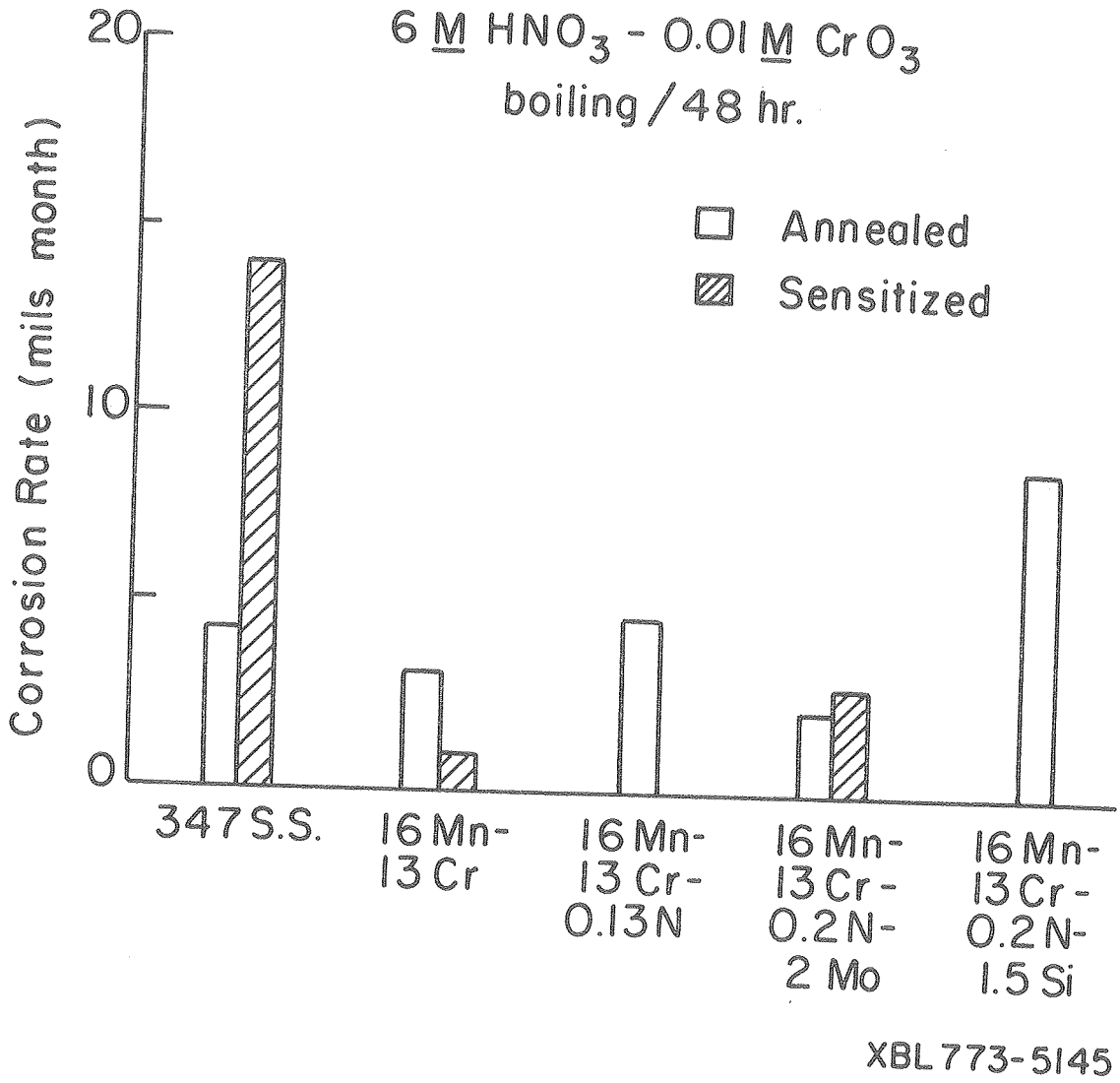
6 M HNO3 - 0.01 M CrO3
boiling / 48 hr.
Annealed
Sensitized
Corrosion Rate (mils month)
20
10
0
347 S.S.
16 Mn-13 Cr
16 Mn-13 Cr-0.13 N
16 Mn-13 Cr-0.2 N-2 Mo
16 Mn-13 Cr-0.2 N-1.5 Si
XBL 773-5145

Figure 14.

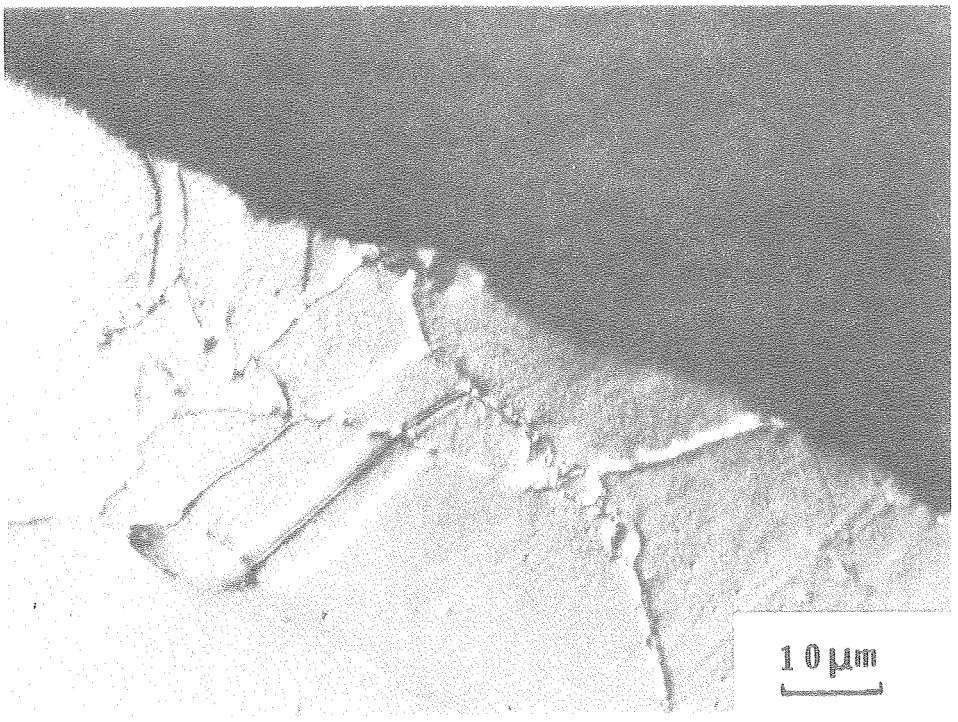

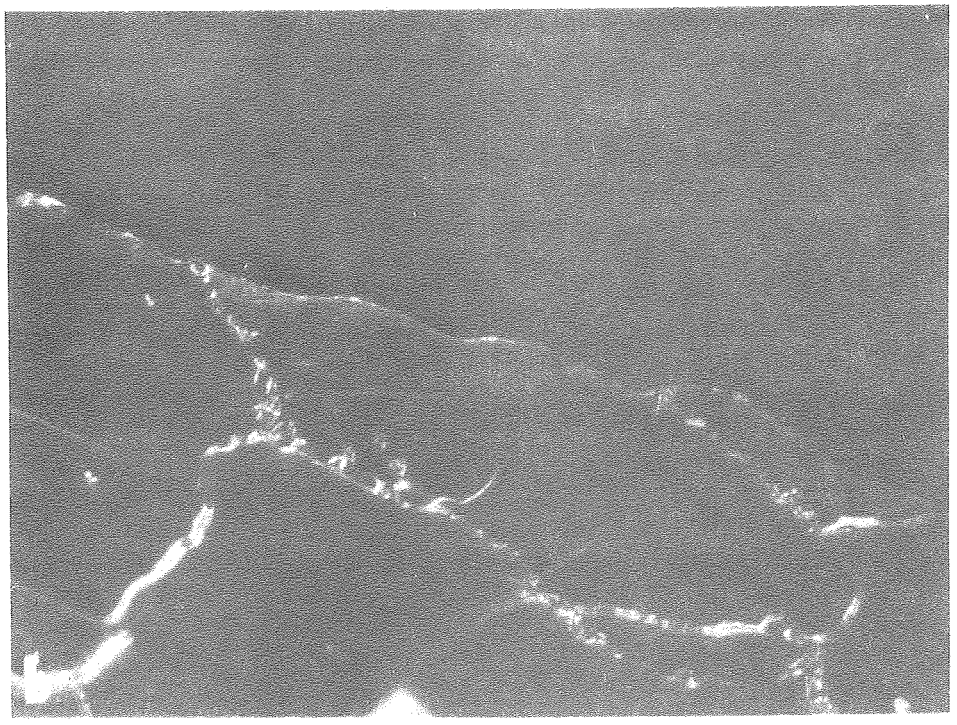

XBB 772-1154

Figure 15.